

Multimerization of an Alcohol Dehydrogenase by Fusion to a Designed Self-Assembling Protein Results in Enhanced Bioelectrocatalytic Operational Stability

Beyza Bulutoglu,^{†,‡} Florika C. Macazo,[‡] Jacob Bale,[§] Neil King,^{§,||} David Baker,^{§,||} Shelley D. Minter,[‡] and Scott Banta^{*,†}

[†]Department of Chemical Engineering, Columbia University, New York, New York 10027, United States

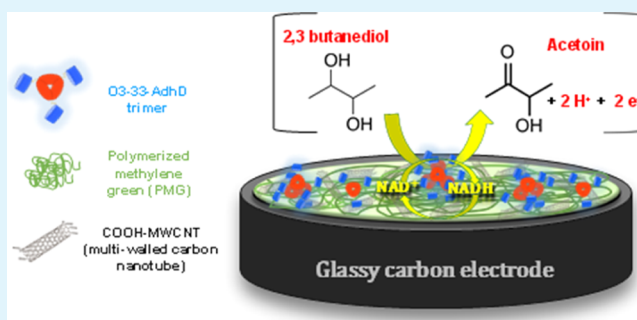
[‡]Department of Chemistry, The University of Utah, Salt Lake City, Utah 84112, United States

[§]Department of Biochemistry and ^{||}Institute for Protein Design, University of Washington, Seattle, Washington 98195, United States

Supporting Information

ABSTRACT: Proteins designed for supramolecular assembly provide a simple means to immobilize and organize enzymes for biotechnology applications. We have genetically fused the thermostable alcohol dehydrogenase D (AdhD) from *Pyrococcus furiosus* to a computationally designed cage-forming protein (O3-33). The trimeric form of the O3-33–AdhD fusion protein was most active in solution. The immobilization of the fusion protein on bioelectrodes leads to a doubling of the electrochemical operational stability as compared to the unfused control proteins. Thus, the fusion of enzymes to the designed self-assembling domains offers a simple strategy to increase the stability in biocatalytic systems.

KEYWORDS: alcohol dehydrogenase D, bioelectrocatalysis, protein self-assembly, protein engineering, enzyme immobilization, operational stability



INTRODUCTION

The application of enzymes in various biotechnology applications is continuing to expand because of their ability to selectively catalyze a range of reactions under mild conditions.^{1–4} A critical challenge in the use of enzymes in many applications is stability. Immobilization methods have been explored as this approach can improve enzyme recycling, and can lead to enhanced stability.^{5–8} Recently, self-assembling protein complexes have been explored for a range of applications including biosensing, drug delivery, imaging, and biocatalysis.^{9–11} These scaffolds can offer unique properties such as high stability, tunable size, biocompatibility,^{12,13} and the opportunity to be decorated with additional biomolecules of interest, such as enzymes. Naturally occurring proteins have been engineered, as well as virus-like particles formed by heterodimeric and homotrimeric coiled-coil bundles,¹⁴ peptide-based self-assembled cages composed of approximately 1500 copies of two types of peptides,¹⁵ and complexes formed by positively supercharged green fluorescent protein fusions and capsids with negatively charged surfaces.¹⁶

Synthetic protein complexes have also been designed in silico, via the creation of de novo protein–protein interfaces.^{17–20} These protein cages can be used to organize molecules in the interior or on the exterior of the assembled complexes, making them promising templates for a variety of

biotechnology applications, including biocatalysis. In this study, a thermostable alcohol dehydrogenase enzyme was genetically fused to a computationally designed cage-forming protein, so that the enzyme would decorate the outside of the cages. This design would provide a simple approach as it is composed of a single self-assembling fusion protein that does not require any further modification for supramolecular coordination.²¹

Alcohol dehydrogenase D (AdhD) is a 34 kDa thermostable monomer from *Pyrococcus furiosus* that belongs to the aldo keto reductase (AKR) superfamily.²² It has a canonical (α/β)₈ barrel structure and broad substrate specificity with highest activity toward secondary alcohols (e.g. 2,3-butanediol) and ketones. AdhD can tolerate high temperatures (up to 100 °C),²³ and use both NAD(H) and NADP(H) as cofactors. Kinetically it follows a reversible ordered bi bi reaction mechanism where the cofactor binds first to the enzyme followed by substrate binding.^{23,24} These features make AdhD a valuable enzyme for industrial biotransformations. Extensive mutational studies have been performed in the cofactor and substrate binding pockets of AdhD to alter its cofactor and

Received: March 8, 2019

Accepted: May 8, 2019

Published: May 8, 2019

substrate specificities.^{25–27} A crystal structure of AdhD has not been solved yet; however, a homology model based on other AKRs is shown in Figure 1A. O3-33 is a mutant version of the

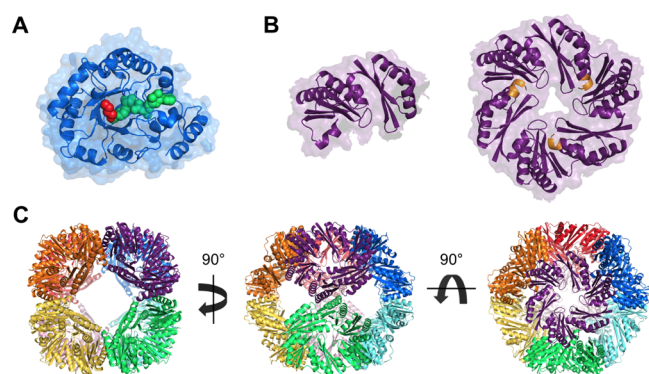


Figure 1. Structures of proteins used to create the fusion protein. (A) Homology model of AdhD bound to its substrate 2,3-butanediol (red) and cofactor NAD⁺ (green). The model was created using prostaglandin F synthase from *Trypanosoma brucei* (1VBJ) as a template. (B) Cage monomer O3-33 (left) and a cage component formed by three subunits (right), with the C-terminus of each monomer highlighted in orange. (C) Quaternary cage structures formed by 24 O3-33 monomers (each trimer is shown in a different color). All cage figures were rendered in PyMOL (PDB file 4DDF).

PduA tandem BMC domain shell protein from *Salmonella enterica*.²⁸ O3-33 was computationally designed to self-assemble into a protein cage formed by 24 subunits with octahedral symmetry.²⁰ The structure of the designed cage-forming monomer O3-33 is shown in Figure 1B. The O3-33 monomer assembles into a homotrimer and eight of these trimers assemble into an octahedral protein cage as shown in Figure 1C.

By fusing the cage-forming monomer O3-33 to AdhD, we created an enzyme-decorated protein assembly. This complex was assessed via kinetic analysis and in an electrochemical system, where O3-33–AdhD protein assembly was used as an anode configuration for biocatalytic oxidation reactions. The results of this study demonstrate the use of designed protein complexes as a means to organize enzyme co-localization, which can benefit many biotechnology applications including biocatalysis.

RESULTS AND DISCUSSION

Construction of O3-33–AdhD. We generated an enzyme/cage monomer of 53 kDa by genetically fusing AdhD to the C-terminus of O3-33 using a flexible glycine–serine linker as explained in the Experimental Section (Figure S1A). This arrangement should allow for the AdhD enzymes to be displayed on the exterior of the self-assembling cage structure (illustrated in Figure S1B,C). A fully assembled cage would display 24 AdhD molecules. Upon expression and purification of the cage-enzyme fusion protein, we obtained fractions from size exclusion chromatography (SEC) that formed a large complex, termed assembly A, and a smaller complex, termed assembly B. Their electrophoretic mobilities were the same on denaturing sodium dodecyl sulfate polyacrylamide gel electrophoresis (SDS-PAGE) gels but distinctively different on blue native PAGE gels, where assembly B migrated faster than assembly A. The apparent molecular weights of the assemblies as well as the unmodified

O3-33 cages determined from the native PAGE gels were inconsistent with calculated values (Figure S2). As native PAGE gels were unreliable, we performed chromatogram analysis and compared the elution profiles of O3-33 by itself, O3-33–AdhD as well as a protein standard composed of six different proteins (Figure S3), in order to understand the assembly state of the fusion protein O3-33–AdhD. It is likely that the fusion of the enzyme, which is larger than the cage monomer (~19 kDa), may introduce steric hindrance to cage formation, leading to the different assembly populations. On the basis of the SEC purification, the large complex is most likely aggregated material, which eluted as a single peak early in the chromatograms (Figures S2 and S3). Assembly B is most likely a trimer, as the location of its elution peak is consistent with the trimeric molecular weight (159 kDa) based on the elution profile of standard protein samples. The two different enzyme assemblies (assembly A and assembly B) were compared via steady-state kinetic analyses and bioelectrocatalysis experiments. Control experiments were also performed with purified AdhD and O3-33 samples that were mixed together but not genetically fused.

Kinetic Analysis of O3-33–AdhD. AdhD follows the ordered bi bi kinetic mechanism. Initial rate reactions were performed at 45 °C in 50 mM glycine buffer (pH 9.3) with varying concentrations of NAD⁺ and 2,3-butanediol. The activity of the large complex (assembly A) was found to be lower than the smaller complex (assembly B) (Figure S4) and full kinetic assays were therefore performed for assembly B only (hereafter, all statements related to the fusion complex refer to the assembly B trimers unless otherwise indicated). The initial rate data were fit globally to eq 1

$$v = \frac{E_t k_{\text{cat}} [A][B]}{K_{iA} K_B + K_B [A] + K_A [B] + [A][B]} \quad (1)$$

where E_t is the total enzyme concentration, k_{cat} is the turnover number, K_{iA} is the cofactor dissociation constant, and K_A and K_B are the Michaelis constants for the cofactor (NAD⁺) and the substrate (2,3-butanediol), respectively. The dissociation constant for the cofactor was previously measured for AdhD to be $37 \pm 2 \mu\text{M}$ and was assumed to be unchanged for the fusion protein.²⁵ The results for the fusion protein complex and the protein mixture, containing equimolar amounts of unfused AdhD and O3-33, are presented in Table 1. Representative enzymatic activities of O3-33–AdhD, O3-33 + AdhD mixed, and O3-33 by itself are shown in Figure S5, where O3-33 did not show any activity under the experimental conditions as expected.

The k_{cat} value of the fusion enzyme decreased approximately by twofold, whereas both Michaelis constants of the fusion

Table 1. Kinetic Parameters of the O3-33–AdhD Fusion Protein Compared to AdhD Mixed with the O3-33 Cage-Forming Protein^a

parameter	O3-33–AdhD	O3-33 + AdhD
K_{iA} (μM)	37 ± 2	37 ± 2
k_{cat} (s^{-1})	0.046 ± 0.002	0.088 ± 0.009
K_A (μM)	140 ± 20	20 ± 7
K_B (mM)	140 ± 10	38 ± 8

^aReactions were performed at 45 °C in 50 mM glycine buffer (pH 9.3), in triplicate. The values are given as means \pm standard deviations.

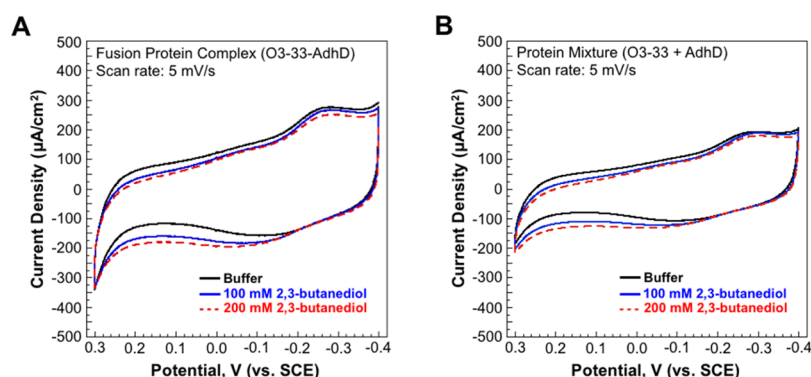


Figure 2. Cyclic voltammograms obtained for the immobilized (A) fusion protein O3-33-AdhD and (B) O3-33 + AdhD protein mixture (O3-33 and AdhD proteins individually expressed and purified, mixed to an equal molar ratio compared to assembly B). Electrochemical oxidation of 2,3-butanediol by immobilized proteins in the presence of 0 mM (black), 100 mM (blue), or 200 mM (red) 2,3-butanediol. Apparent turnover numbers (TON_{app}) approximated from the CV's are 0.0084 ± 0.0001 and $0.0086 \pm 0.0002 \text{ s}^{-1}$ for the O3-33-AdhD complex and O3-33 + AdhD protein mixture, respectively.

protein were increased compared to the unfused and mixed protein control group. The K_A value (Michaelis constant for the cofactor) increased by sevenfold, whereas the K_B value (Michaelis constant for the substrate) showed a fourfold increase. Thus, although the assembly B trimers were more active than those of assembly A, the genetic fusion of the O3-33 protein to the N-terminus of the AdhD enzyme led to a decrease in the AdhD kinetic activity. This was unexpected as the N-terminus is on the other side of the $(\alpha/\beta)_8$ barrel from the active site and prior fusions to the N-terminus have not affected AdhD activity.²⁹ Many groups have noted with other proteins that immobilization can lead to detrimental impacts in activity.^{5,30,31} It is not clear from these data whether multimer formation impacts the structure of the AdhD enzyme, but this seems unlikely because of the high degree of structural stability of the protein (both high temperatures and guanidine HCl are required for denaturation). There is an increasing appreciation that biomolecular fusions near active sites alter local micro-environments, leading to impacts on catalytic activity,³² and these effects may also explain the observed reduction in catalysis.

Electrochemical Activity of O3-33-AdhD. The activity of the O3-33-AdhD fusion protein complex trimers was measured electrochemically by immobilizing the complexes on glassy carbon (GC) electrodes with methylene green (MG)-modified multiwalled carbon nanotubes (MWCNTs), poly-ethylenimine hydrogel, and the cross-linker ethylene glycol diglycidyl ether (EGDGE). This forms a stable hydrogel composite of a covalently linked polymer, an enzyme, and MWCNTs.^{33,34} The MWCNTs provide high surface area, thus increasing the overall electrical conductivity of the system.³⁵⁻³⁹ MG was incorporated as an electrocatalyst for NADH oxidation.^{33,40,41} All cyclic voltammograms (CVs) reported herein were produced in the presence of 5 mM NAD^+ and 100–200 mM 2,3-butanediol unless otherwise stated. As shown in Figure 2A, the CVs obtained for the fusion protein complex showed increased current densities in the presence of 100 mM (Figure 2A, blue solid curve; $160 \pm 20 \mu\text{A cm}^{-2}$) and 200 mM (Figure 2A, red dashed curve; $180 \pm 30 \mu\text{A cm}^{-2}$) 2,3-butanediol, with an onset potential of -0.10 V , whereas a protein-free control showed no catalytic activity in the presence of the cofactor and the substrate (Figure S6). This is consistent with oxidation of 2,3-butanediol by NAD^+ forming NADH, which is then re-oxidized at the poly(MG)

electrode to regenerate NAD^+ . The current measured is directly proportional to the NADH being oxidized.

CVs were also produced for the mixtures of unfused AdhD and O3-33 combined in equimolar amounts (Figure 2B), and similar bioelectrocatalytic waves were observed in the presence of 100 mM ($110 \pm 10 \mu\text{A cm}^{-2}$) and 200 mM 2,3-butanediol ($130 \pm 10 \mu\text{A cm}^{-2}$) at -0.10 V . In contrast to the kinetic assay results, the catalytic oxidative current densities observed for the fusion complex were generally higher than the O3-33 + AdhD mixture in the presence of 2,3-butanediol.

From the CVs obtained in Figure 2, we estimated the apparent turnover numbers (TON_{app}) for the O3-33-AdhD fusion complex and O3-33 + AdhD protein mixture (Table 2),

Table 2. Approximated Electrochemical Kinetic Parameters of the O3-33-AdhD Fusion Protein Complex (Assembly B) and AdhD Mixed with the O3-33 Cage-Forming Protein^a

parameter	O3-33-AdhD	O3-33 + AdhD
J_{max} ($\mu\text{A cm}^{-2}$)	7.2 ± 0.3	4.5 ± 0.1
K_B (mM)	28 ± 4	27 ± 3
TON_{app} (s^{-1})	0.0084 ± 0.0001	0.0086 ± 0.0002

^a J_{max} is the maximum current density obtained at saturating concentrations of the substrate, K_B is the apparent Michaelis constant for the substrate (0–1000 mM 2,3-butanediol; 5 mM NAD^+), TON_{app} is the apparent turnover number approximated from the CVs (Figure 2; 5 mV sec^{-1} scan rate; 100 mM 2,3-butanediol; 5 mM NAD^+). Reactions were performed at 25 °C in 50 mM glycine, 200 mM NaCl buffer (pH 9.3), in triplicate. The values are given as means \pm standard deviations.

taking into account the total amount of charge (Q_T) (C) generated for each complex with and without the substrate at a sample interval of 0.20 s, the electroactive surface coverage (mol cm^{-2}), and the electrode surface area (0.0707 cm^2). Approximated total turnover numbers extrapolated from the CVs are 0.0084 ± 0.0001 and $0.0086 \pm 0.0002 \text{ s}^{-1}$ for the O3-33-AdhD fusion and O3-33 + AdhD mixture proteins, respectively. These bioelectrocatalytic TON_{app} values are substantially lower than the k_{cat} values obtained via the steady-state kinetic analysis of the protein complex in solution (Table 1).

In these experiments, multiple steps are taking place. Reactants must diffuse to the enzymatic active sites, catalysis takes place, and cofactors are electrochemically reduced. The

similar values of the fused and unfused enzymes suggest that the differences in the kinetic rates are not rate-limiting in this system. In other words, the decreased kinetic behavior of the fused enzyme does not lead to decreased bioelectrocatalysis, suggesting that one of the other mechanistic processes is rate-limiting. It is likely that the immobilization of the enzymes leads to transport limitations such that the diffusion of reactants to or from the enzymes or electrodes limits the activity of both electrode configurations.³⁴

The attribution of similar bioelectrode performances to mass transport limitations are consistent with our previous results in the engineering of AdhD to use an alternative cofactor, nicotinamide mononucleotide (NMN⁺). We previously showed similar bioanode performance with NMN(H) and NAD(H) as cofactors despite four orders of difference in the kinetic rate parameters of the enzyme with these cofactors, indicating that transport limitations govern the activity as opposed to kinetic limitations in these systems.

Constant Potential Amperometry Measurements. To further explore the bioelectrocatalytic ability of the fusion protein, constant potential amperometry experiments were carried out at a potential of 0.10 V versus saturated calomel electrode (SCE). Figure 3 shows amperometric titration curves

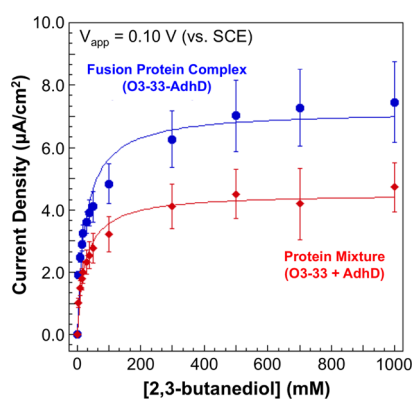


Figure 3. Amperometric titration curves of the immobilized fusion protein complexes (blue curve) and protein mixture (red curve) with 0–1000 mM 2,3-butanediol and 5 mM NAD⁺ ($V_{app} = 0.10$ V). Data points were fitted using the Michaelis–Menten equation.

for the immobilized O3-33–AdhD trimeric fusion (blue curve) and the unfused O3-33 + AdhD mixture (red curve) with 0–1000 mM 2,3-butanediol and 5 mM NAD⁺. The data were fit to the Michaelis–Menten equation to estimate the maximum current densities (J_{max}) and apparent Michaelis constants (K_B) for the substrate (Table 2). The apparent K_B value obtained via amperometry for the fusion protein (28 ± 4 mM) was 20% of the value obtained using steady-state solution kinetics (140 ± 20 mM), whereas the K_B value for the unfused protein mixture obtained via amperometry (28 ± 3 mM) was more similar to the value obtained from kinetic analysis (20 ± 7 mM).

Potentiostatic Stability of O3-33–AdhD. Finally, we explored the changes in operational stability that result from the formation of the fusion protein. Operational stability is a critical potential limitation in biocatalytic systems as the enzymes can denature and degrade during continuous operation.^{42–44} We hypothesized that fusion of AdhD to the self-assembling protein would lead to increased stability of the enzyme, thus increasing the operational stability in a bioelectrocatalysis application. To explore this hypothesis, we

performed a potentiostatic stability test, which is a more rigorous stability test compared to galvanostatic tests, on the O3-33–AdhD trimeric fusion by subjecting the immobilized catalysts to an 8 h constant application of potential (0.10 V vs SCE) in the presence of 1000 mM 2,3-butanediol and 5 mM NAD⁺, while continuously stirring and measuring the resulting current (Figure 4). The resulting currents are given in terms of

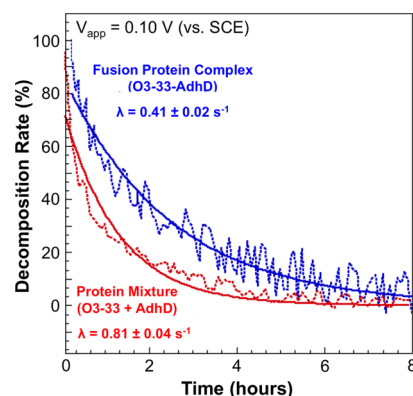


Figure 4. Potentiostatic stability experiments with the fusion protein complexes and mixture of unfused proteins. Amperometric decay rates obtained for the O3-33–AdhD complex (blue curve) and O3-33 + AdhD mixture (red curve) are 0.41 ± 0.02 and 0.81 ± 0.04 s⁻¹, respectively, in the presence of 1000 mM 2,3-butanediol and 5 mM NAD⁺ ($V_{app} = 0.10$ V).

percent decomposition rates, using the initially measured current at the time of substrate addition (1000 mM) as baseline (100%) and calculating the decrease in current over the course of 8 h. Likewise, a comparative current–time curve was also produced for the unfused protein mixture and overlaid in Figure 4 (red curve). The data clearly illustrate the difference in operational stability of the fused and unfused protein complexes. The fusion protein retained ~78% of its activity in the first 30 min, ~41% after 2 h, and ~8% after 5 h (Figure 4, blue curve). In contrast, the unfused O3-33 + AdhD mixture lost almost half of its activity in the first 30 min (~45%), maintained ~17% of its activity after 2 h, and ~2% after 5 h (Figure 4, red curve). Using an exponential decay fit (solid curves in Figure 4), the decay rates obtained for the fusion complex and the mixed control proteins were 0.41 ± 0.02 and 0.81 ± 0.04 s⁻¹, respectively, further demonstrating the enhanced operational stability afforded by the genetic fusion of AdhD to a designed, multimeric protein. It is likely that the oligomerization of the protein complex stabilizes the AdhD enzyme and reduces denaturation of the enzyme in the electrode configuration over time. The same analysis for assembly A (Figure S7) showed that both assemblies showed similar operational stability enhancements.

EXPERIMENTAL SECTION

Plasmids, Chemicals, and Materials. Sodium chloride, glycine, guanidine-hydrochloride (GdnHCl), MG, nicotinamide adenine dinucleotide (NAD⁺), and 2,3-butanediol were purchased from Sigma-Aldrich and used as received. EGDGE was purchased from Polysciences Inc., and carboxyl-functionalized MWCNTs (COOH-MWCNTs) were purchased from Cheap Tubes Inc. Octyl-modified linear poly(ethylenimine) (C8-LPEI) was synthesized following a previously reported procedure.⁴⁵ Isopropyl β-D-1-thiogalactopyranoside (IPTG), ampicillin sodium salt, and kanamycin were purchased from Gold Biotechnology. Amicon centrifugal filters were purchased

from Millipore. SDS-PAGE, native PAGE gels and running buffers were purchased from Invitrogen-Life Technologies. Restriction enzymes and phusion high-fidelity DNA polymerase were purchased from New England Biolabs. *E. coli* BL21(DE3) cell lines were purchased from Biotline. All other reagents and materials were purchased from Sigma-Aldrich (St. Louis, MO) unless otherwise stated.

Construction of the Fusion Plasmid. The construction of the plasmid coding for the wild-type AdhD was described previously.²⁵ The wild-type AdhD gene was inserted into the pET29b-O3-33 plasmid²⁰ (which encodes the O3-33 designed protein) via the *Xho*I restriction site, which resulted in pET29b-O3-33-AdhD-6xhis. The gene coding for AdhD was amplified with the following primers: forward—5' ATTAATACTCGAGGGCGGCGG-CAGCGGCGGCGGCGGAGCGGGCGGCGGCGGAGCATGG-CAAACGCGTGAATGCATTTAACG 3'; reverse—5' TTAAATCTCGAGAAGCTTGTCCACGGAGCTCGAATT C 3'. The base pairs in bold indicate the *Xho*I restriction sites and the underlined sequence introduced a 12-amino acid residue long glycine-serine linker between the proteins. The resulting plasmid was transformed into BL21(DE3) cells for expression. The full protein sequence of the constructed cage fusion protein is given in Table S1. The sequences of all constructs were confirmed via sequencing services provided by Genewiz Inc. (Cambridge, MA).

Expression and Purification of Proteins. All proteins were expressed in 1 L cultures of sterilized Terrific broth (24 g yeast extract, 12 g tryptone, 4 g glycerol, 2.3 g KH₂PO₄, 16.4 g K₂HPO₄ in 1 L deionized water), inoculated with 10 mL overnight cultures. For AdhD, the media was supplemented with 100 μg/mL ampicillin. Kanamycin (50 μg/mL) was added to O3-33 and O3-33-AdhD cultures. The cells were grown to an OD₆₀₀ of 0.6 while shaking at 37 °C, and protein expression was induced with 0.5 mM IPTG. Expression was carried out for 18–20 h at 25 °C, for O3-33 and for the fusion protein. Cells expressing AdhD were incubated at 37 °C, overnight. Cells were harvested by centrifugation at 5000g for 10 min. AdhD pellets were resuspended in 35 mL of size exclusion buffer (20 mM Tris-HCl, 100 mM NaCl, pH 7.4) per L of culture. Cell suspensions were incubated in a water bath at 80 °C for 1 h followed by centrifugation at 15 000g for 30 min. The soluble fractions were collected and concentrated via Amicon filters with 30 kDa molecular weight cutoff. The concentrated samples were loaded onto SEC columns and purified fractions were combined for further investigation. O3-33 and O3-33-AdhD pellets were resuspended in 50 mL of HisTrap binding buffer (20 mM Tris-HCl, 150 mM NaCl and 20 mM imidazole, pH 7.4) per L of culture. Soluble proteins were collected via centrifugation at 15 000g for 30 min after the cells were lysed by sonication with an ultrasonication probe in an ice bath for 6 min (5 s on pulse and 2 s off pulse). The proteins were purified by immobilized metal affinity chromatography using HisTrap columns (GE Healthcare Life Sciences), where bound enzymes were eluted with the elution buffer (20 mM Tris-HCl, 150 mM NaCl, 500 mM imidazole, pH 7.4). Purified O3-33 fractions were used without further purification. O3-33-AdhD fractions were combined, concentrated, and buffer-exchanged into 25 mM Tris-HCl, 200 mM NaCl, pH 8.0. The concentrated samples were loaded onto the SEC column (HiLoad Superdex 16/600200 prep grade from GE Healthcare) and purified fractions were combined for further investigation. For the rest of the experiments, the protein concentrations were determined by measuring the absorbance at 280 nm and using the following extinction coefficients for O3-33, AdhD and O3-33-AdhD: 15 470, 52 370 and 67 840 M⁻¹ cm⁻¹, respectively.

Activity Assays. The activity of the O3-33-AdhD fusion protein was measured in the oxidative direction with different substrate and cofactor concentrations, in 50 mM glycine buffer (pH 9.3) in a 96-well plate. 2,3-Butanediol and NAD⁺ concentrations were varied from zero to 400 and 1 mM, respectively. 280 μL of the substrate solution and 10 μL of the enzyme solution in the assay buffer were incubated at 45 °C for 20 min. The reaction was initiated by the addition of 10 μL of the cofactor solution. The final concentration of O3-33-AdhD

in the assay mixture was 0.693 μM. NADH concentrations were measured spectrophotometrically at 340 nm using the extinction coefficient 6220 M⁻¹ cm⁻¹. O3-33 and AdhD proteins, individually expressed and purified, were mixed to an equal molar ratio for comparison to the fusion protein (one molecule of fusion protein per one molecule of enzyme). The activity of this mixed sample was measured in a similar way as described above where 2,3-butanediol and NAD⁺ concentrations were varied from zero to 100 and 0.2 mM, respectively. The final enzyme concentration used in the kinetic assays of the mixed sample was 0.1 μM. Data were collected in triplicate. In order to estimate the steady-state kinetic parameters, initial rate data were fit to the ordered bi bi equation (eq 1) using nonlinear least-squares regression via Igor Pro software.

Electrode Surface Modification. Modification of the electrode surfaces was carried out at 25 °C using 3 mm GC electrodes (CH Instruments). The electrodes were mechanically polished in an aluminum oxide-containing micropolish (Buehler) and thoroughly rinsed with ultrapure water, air-dried, and utilized for subsequent modifications. Protein immobilization on GC electrodes was carried out following a previously reported protocol with modifications.³³ Two milligrams of COOH-MWCNT was added to a 67.5 μL C8LPEI (10 mg/mL) solution and vortexed for 5 s, sonicated for 30 s, and the vortex/sonication cycle was repeated three times. In a separate tube, 2.88 μL of MG (1.15 mM) was added to either the mixture (O3-33 + AdhD) or the fusion (O3-33-AdhD) proteins (total protein concentration is 3 mg/mL) and vortexed for 5 s. This MG/protein mixture was added to the solution containing the COOH-MWCNT and C8LPEI and vortexed for 5 s. To this final solution, 4.05 μL of EGDGE (10% v/v) was added and the mixture was vortexed for 5 s and sonicated for 30 s. The resulting mixtures were coated onto GC electrodes by adding 3 μL of the mixture and distributing evenly across the electrode surface using a pipette tip. The MWCNT/MG/O3-33-AdhD-modified electrodes were air-dried and allowed to cure at 4 °C for 2 h prior to use. Protein-free controls were also prepared using the same immobilization protocol in the absence of the proteins.

Electrochemical Measurements and Data Analysis. Electrochemical measurements were performed using cyclic voltammetry (CV) on a CH Instruments 611C Electrochemical Work Station (CH Instruments), employing a step potential of 0.001 V, a potential range of -0.40–0.30 V (vs SCE), and a scan rate of 5 mV/s, unless otherwise specified. A three-electrode setup with an enzyme-modified working electrode, SCE reference electrode, and platinum mesh counter electrode, was utilized in a 3 mL glass cell containing 50 mM glycine, 200 mM NaCl buffer, pH 9.3. All amperometric titrations were performed via constant potential amperometry using the same three-electrode setup with the potential held at 0.10 V (vs SCE) in 50 mM glycine, 200 mM NaCl buffer, pH 9.3. The amperometric currents generated for the substrate-induced oxidation were utilized for data analyses, where the values were normalized to the electrode area (0.0707 cm²) and expressed as current density ± standard error of mean (SEM) in units of mA/cm². The error bars reported represent the SEM made on three different electrodes. All positive negative currents correspond to oxidations.

CONCLUSIONS

In conclusion, we created an enzyme-decorated protein assembly by genetically fusing the AdhD alcohol dehydrogenase to the de novo designed O3-33 octahedral cage-forming protein, and demonstrated its application in biocatalytic oxidation reactions. It appears that the fusion of AdhD to O3-33 disrupted the formation of the protein cage in solution, and it is not clear whether the designed protein cages were more likely to form upon immobilization on the electrodes. Further structural studies may shed light on how the addition of AdhD affected the oligomeric state of the cage assemblies. However, the steady-state kinetic results indicate that trimeric complexes are more active than the larger (possibly aggregated) species, although the trimers were less active

than the unfused control enzymes. Despite the loss of kinetic activity, in immobilized bioelectrocatalytic studies, similar turnover numbers suggest that these systems (fused and unfused complexes) are limited by mass transfer and not kinetic activity. The fusion of AdhD to the O3-33 self-assembling protein approximately doubled the operational stability of the immobilized thermostable AdhD enzyme. Although the protein fusions do not appear to form the anticipated 24-mer protein cage structures in solution, the fusion of the enzyme to the self-assembling domains demonstrates the value of using designed protein complexes as a simple means to organize enzymatic activity, which leads to enhanced operational stability that could be impactful for many different biotechnology applications such as biosensors, consumer products, environmental remediation, and industrial catalysis.

■ ASSOCIATED CONTENT

Supporting Information

The Supporting Information is available free of charge on the ACS Publications website at DOI: 10.1021/acsami.9b04256.

Cartoon rendering of the constructed fusion protein and cage-assembly; SDS-PAGE and native-PAGE analyses of O3-33-AdhD and O3-33; SEC chromatography data of O3-33-AdhD, protein standards, and O3-33; comparative spectrophotometric kinetic data; enzymatic activities of O3-33, O3-33-AdhD fusion protein, and O3-33 + AdhD protein mixture; CVs obtained for the immobilized protein-free control when challenged with 2,3-butanediol and NAD⁺; potentiostatic stability experiments with assemblies A and B; and protein primary sequence of the O3-33-AdhD fusion protein (PDF)

■ AUTHOR INFORMATION

Corresponding Author

*E-mail: sbanta@columbia.edu.

ORCID

Beyza Bulutoglu: 0000-0002-4435-413X

Florika C. Macazo: 0000-0001-6706-2407

Shelley D. Minter: 0000-0002-5788-2249

Scott Banta: 0000-0001-7885-0150

Present Address

[†]Center for Engineering in Medicine, Harvard Medical School and Massachusetts General Hospital, Boston, MA 02114, USA.

Author Contributions

B.B. and F.C.M. contributed equally. D.B., S.M., and S.B. developed the initial concept. J.B., N.K., and D.B. provided the O3-33 protein and suggested the location of AdhD fusion on O3-33. B.B., F.C.M., S.M., and S.B. designed the experiments. B.B. and F.C.M. performed the experiments. B.B., F.C.M., S.M., and S.B. wrote the article. All the authors commented on the article and have given approval to the final version of the article.

Notes

The authors declare no competing financial interest.

■ ACKNOWLEDGMENTS

This work was supported by the U.S. Air Force Office of Scientific Research (FA9550-12-1-0112) and the US Army Research Office through the Department of Defense Multi-

disciplinary University Research Initiative (MURI) Program (W911NF1410263).

■ REFERENCES

- (1) Choi, J.-M.; Han, S.-S.; Kim, H.-S. Industrial Applications of Enzyme biocatalysis: Current Status and Future Aspects. *Biotechnol. Adv.* **2015**, *33*, 1443–1454.
- (2) Chapman, J.; Ismail, A. E.; Dinu, C. Z. Industrial Applications of Enzymes: Recent Advances, Techniques, and Outlooks. *Catalyst* **2018**, *8*, 238.
- (3) Jemli, S.; Ayadi-Zouari, D.; Hlima, H. B.; Bejar, S. Biocatalysts: Application and Engineering for Industrial Purposes. *Crit. Rev. Biotechnol.* **2014**, *36*, 246–258.
- (4) Porter, J. L.; Rusli, R. A.; Ollis, D. L. Directed Evolution of Enzymes for Industrial Biocatalysis. *ChemBioChem* **2015**, *17*, 197–203.
- (5) Mohamad, N. R.; Marzuki, N. H. C.; Buang, N. A.; Huyop, F.; Wahab, R. A. An Overview of Technologies for Immobilization of Enzymes and Surface Analysis Techniques for Immobilized Enzymes. *Biotechnol. Biotechnol. Equip.* **2015**, *29*, 205–220.
- (6) Datta, S.; Christena, L. R.; Rajaram, Y. R. S. Enzyme Immobilization: An Overview on Techniques and Support Materials. *3 Biotech* **2013**, *3*, 1–9.
- (7) DiCosimo, R.; McAuliffe, J.; Poulou, A. J.; Bohlmann, G. Industrial Use of Immobilized Enzymes. *Chem. Soc. Rev.* **2013**, *42*, 6437–6474.
- (8) Jia, F.; Narasimhan, B.; Mallapragada, S. Materials-Based Strategies for Multi-Enzyme Immobilization and Co-localization: A Review. *Biotechnol. Bioeng.* **2013**, *111*, 209–222.
- (9) Glasgow, J.; Tullman-Ercek, D. Production and Applications of Engineered Viral Capsids. *Appl. Microbiol. Biotechnol.* **2014**, *98*, 5847–5858.
- (10) Sun, Q.; Chen, Q.; Blackstock, D.; Chen, W. Post-Translational Modification of Bionanoparticles as a Modular Platform for Biosensor Assembly. *ACS Nano* **2015**, *9*, 8554–8561.
- (11) Li, K.; Zhang, Z.-P.; Luo, M.; Yu, X.; Han, Y.; Wei, H.-P.; Cui, Z.-Q.; Zhang, X.-E. Multifunctional Ferritin Cage Nanostructures for Fluorescence and MR Imaging of Tumor Cells. *Nanoscale* **2012**, *4*, 188–193.
- (12) Li, F.; Gao, D.; Zhai, X.; Chen, Y.; Fu, T.; Wu, D.; Zhang, Z.-P.; Zhang, X.-E.; Wang, Q. Tunable, Discrete, Three-Dimensional Hybrid Nanoarchitectures. *Angew. Chem., Int. Ed.* **2011**, *50*, 4202–4205.
- (13) Zhang, S. Fabrication of Novel Biomaterials Through Molecular Self-Assembly. *Nat. Biotechnol.* **2003**, *21*, 1171–1178.
- (14) Fletcher, J. M.; Harniman, R. L.; Barnes, F. R. H.; Boyle, A. L.; Collins, A.; Mantell, J.; Sharp, T. H.; Antognozzi, M.; Booth, P. J.; Linden, N.; Sessions, R. B.; Verkade, P.; Woolfson, D. N. Self-Assembling Cages from Coiled-Coil Peptide Modules. *Science* **2013**, *340*, 595–599.
- (15) Ross, J. F.; Bridges, A.; Fletcher, J. M.; Shoemark, D.; Alibhai, D.; Bray, H. E. V.; Beesley, J. L.; Dawson, W. M.; Hodgson, L. R.; Mantell, J.; Verkade, P.; Edge, C. M.; Sessions, R. B.; Tew, D.; Woolfson, D. N. Decorating Self-Assembled Peptide Cages with Proteins. *ACS Nano* **2017**, *11*, 7901–7914.
- (16) Azuma, Y.; Zschoche, R.; Tinzl, M.; Hilvert, D. Quantitative Packaging of Active Enzymes into a Protein Cage. *Angew. Chem., Int. Ed. Engl.* **2016**, *55*, 1531–1534.
- (17) Raeeszadeh-Sarmazdeh, M.; Hartzell, E.; Price, J. V.; Chen, W. Protein Nanoparticles as Multifunctional Biocatalysts and Health Assessment Sensors. *Curr. Opin. Chem. Eng.* **2016**, *13*, 109–118.
- (18) Bale, J. B.; Gonen, S.; Liu, Y.; Sheffler, W.; Ellis, D.; Thomas, C.; Cascio, D.; Yeates, T. O.; Gonen, T.; King, N. P.; Baker, D. Accurate Design of Megadalton-Scale Two-Component Icosahedral Protein Complexes. *Science* **2016**, *353*, 389–394.
- (19) Sciore, A.; Su, M.; Koldewey, P.; Eschweiler, J. D.; Diffley, K. A.; Linhares, B. M.; Ruotolo, B. T.; Bardwell, J. C. A.; Skiniotis, G.; Marsh, E. N. G. Flexible, Symmetry-Directed Approach to Assembling Protein Cages. *Proc. Natl. Acad. Sci. U.S.A.* **2016**, *113*, 8681–8686.

- (20) King, N. P.; Sheffler, W.; Sawaya, M. R.; Vollmar, B. S.; Sumida, J. P.; Andre, I.; Gonen, T.; Yeates, T. O.; Baker, D. Computational Design of Self-Assembling Protein Nanomaterials with Atomic Level Accuracy. *Science* **2012**, *336*, 1171–1174.
- (21) Kobayashi, N.; Arai, R. Design and Construction of Self-Assembling Supramolecular Protein Complexes Using Artificial and Fusion Proteins as Nanoscale Building Blocks. *Curr. Opin. Biotechnol.* **2017**, *46*, 57–65.
- (22) Ma, K.; Adams, M. W. W. An Unusual Oxygen-Sensitive, Iron- and Zinc-Containing Alcohol Dehydrogenase from the Hyperthermophilic Archaeon *Pyrococcus furiosus*. *J. Bacteriol.* **1999**, *4*, 1163–1170.
- (23) Machielsen, R.; Uria, A. R.; Kengen, S. W. M.; van der Oost, J. Production and Characterization of a Thermostable Alcohol Dehydrogenase that Belongs to the Aldo-Keto Reductase Superfamily. *Appl. Environ. Microbiol.* **2006**, *72*, 233–238.
- (24) Solanki, K.; Abdallah, W.; Banta, S. Extreme makeover: Engineering the Activity of a Thermostable Alcohol Dehydrogenase (AdhD) from *Pyrococcus furiosus*. *Biotechnol. J.* **2016**, *11*, 1483–1497.
- (25) Campbell, E.; Wheeldon, I. R.; Banta, S. Broadening the Cofactor Specificity of a Thermostable Alcohol Dehydrogenase Using Rational Protein Design Introduces Novel Kinetic Transient Behavior. *Biotechnol. Bioeng.* **2010**, *107*, 763–774.
- (26) Campbell, E.; Chuang, S.; Banta, S. Modular Exchange of Substrate-Binding Loops Alters Both Substrate and Cofactor Specificity in a Member of the Aldo-Keto Reductase Superfamily. *Protein Eng., Des. Sel.* **2013**, *26*, 181–186.
- (27) Solanki, K.; Abdallah, W.; Banta, S. Engineering the cofactor specificity of an alcohol dehydrogenase via single mutations or insertions distal to the 2'-phosphate group of NADP(H). *Protein Eng., Des. Sel.* **2017**, *30*, 373–380.
- (28) Crowley, C. S.; Cascio, D.; Sawaya, M. R.; Kopstein, J. S.; Bobik, T. A.; Yeates, T. O. Structural Insight into the Mechanisms of Transport across the *Salmonella enterica* Pdu Microcompartment Shell. *J. Biol. Chem.* **2010**, *285*, 37838–37846.
- (29) Wheeldon, I. R.; Campbell, E.; Banta, S. A Chimeric Fusion Protein Engineered with Disparate Functionalities-Enzymatic Activity and Self-assembly. *J. Mol. Biol.* **2009**, *392*, 129–142.
- (30) Hanefeld, U.; Gardossi, L.; Magner, E. Understanding Enzyme Immobilisation. *Chem. Soc. Rev.* **2009**, *38*, 453–468.
- (31) Homaei, A. A.; Sari, R.; Vianello, F.; Stevanator, R. Enzyme Immobilization: An Update. *J. Chem. Biol.* **2012**, *6*, 185–205.
- (32) Lancaster, L.; Abdallah, W.; Banta, S.; Wheeldon, I. Engineering Enzyme Microenvironments for Enhanced Biocatalysis. *Chem. Soc. Rev.* **2018**, *47*, 5177–5186.
- (33) Meredith, M. T.; Giroud, F.; Minteer, S. D. Azine/Hydrogel/Nanotube Composite-Modified Electrodes for NADH Catalysis and Enzyme Immobilization. *Electrochim. Acta* **2012**, *72*, 207–214.
- (34) Macazo, F. C.; Hickey, D. P.; Abdellaoui, S.; Sigman, M. S.; Minteer, S. D. Polymer-Immobilized, Hybrid Multi-Catalyst Architecture for Enhanced Electrochemical Oxidation of Glycerol. *Chem. Commun.* **2017**, *53*, 10310–10313.
- (35) Cosnier, S.; Holzinger, M.; Le Goff, A. Recent Advances in Carbon Nanotube-Based Enzymatic Fuel Cells. *Front. Bioeng. Biotechnol.* **2014**, *2*, 45.
- (36) Zebda, A.; Gondran, C.; Le Goff, A.; Holzinger, M.; Cinquin, P.; Cosnier, S. Mediatorless High-Power Glucose Biofuel Cells Based on Compressed Carbon Nanotube-Enzyme Electrodes. *Nat. Commun.* **2011**, *2*, 370.
- (37) Meredith, M. T.; Minteer, S. D. Biofuel Cells: Enhanced Enzymatic Bioelectrocatalysis. *Annu. Rev. Anal. Chem.* **2012**, *5*, 157–179.
- (38) Handa, Y.; Yamagiwa, K.; Ikeda, Y.; Yanagisawa, Y.; Watanabe, S.; Yabuuchi, N.; Komaba, S. Fabrication of Carbon-Felt-Based Multi-Enzyme Immobilized Anodes to Oxidize Sucrose for Biofuel Cells. *ChemPhysChem* **2014**, *15*, 2145–2151.
- (39) Kowalewska, B.; Kulesza, P. J. Toward More Efficient Bioelectrocatalytic Oxidation of Ethanol for Amperometric Sensing and Biofuel Cell Technology. *Anal. Chem.* **2012**, *84*, 9564–9571.
- (40) Campbell, E.; Meredith, M.; Minteer, S. D.; Banta, S. Enzymatic Biofuel Cells Utilizing a Biomimetic Cofactor. *Chem. Commun.* **2012**, *48*, 1898–1900.
- (41) Akers, N. L.; Moore, C. M.; Minteer, S. D. Development of Alcohol/O₂ Biofuel Cells Using Salt-Extracted Tetrabutylammonium Bromide/Nafion Membranes to Immobilize Dehydrogenases Enzymes. *Electrochim. Acta* **2005**, *50*, 2521–2525.
- (42) Shrier, A.; Giroud, F.; Rasmussen, M.; Minteer, S. D. Operational Stability Assays for Bioelectrodes for Biofuel Cells: Effect of Immobilization Matrix on Laccase Biocathode Stability. *J. Electrochem. Soc.* **2014**, *161*, H244–H248.
- (43) Jenkins, P. A.; Boland, S.; Kavanagh, P.; Leech, D. Evaluation of Performance and Stability of Biocatalytic Redox Films Constructed with Different Copper Oxygenases and Osmium-Based redox Polymers. *Bioelectrochemistry* **2009**, *76*, 162–168.
- (44) Barton, S. C.; Galloway, J.; Atanassov, P. Enzymatic Biofuel Cells for Implantable and Microscale Devices. *Chem. Rev.* **2004**, *104*, 4867–4886.
- (45) Moehlenbrock, M. J.; Meredith, M. T.; Minteer, S. D. Bifunctional Polyamines for the Aqueous Dispersion of Carbon Nanotubes and the Formation of Carbon Nanotube-Impregnated Hydrogel Composites. *MRS Commun.* **2011**, *1*, 37–40.